Photochemical & Photobiological Sciences (2026) 25:47–59
https://doi.org/10.1007/s43630-025-00823-7

RESEARCH

A study on the impact of betalain chemical modification on the efficiency and stability of dye-sensitized solar cells

Aziza Chabou[1] · Benamar Cheknane[1] · Zakia Zeffouni[1,2] · Faiza Zermane[1] · Massimiliano Cordaro[3] · Mariangela Latino[4] · Ilaria Citro[4] · Donatella Spadaro[4] · Stefano Trocino[5] · Giuseppe Calogero[4]

Received: 18 June 2025 / Accepted: 19 November 2025 / Published online: 15 December 2025

Abstract
This study investigates the effect of the chemical modification of betalain pigments, extracted from purple *Bougainvillea glabra*, on the photovoltaic performance of dye-sensitized solar cells (DSSCs). The extraction yield of crude betacyanin from *B. glabra* was approximately 8.75%. The unmodified betalain (B) and the modified betalain (MB) were used as natural sensitizers; their adsorption behaviors on TiO_2 were analyzed and compared. The structural and optical properties of both dyes were characterized using Fourier-transform infrared (FTIR) spectroscopy, proton nuclear magnetic resonance (^{1}H-NMR) spectroscopy, and ultraviolet-visible (UV–Vis) spectroscopy. The chemical modification of the crude betacyanin extract proceeded with a yield of 69.5%. The photovoltaic performance of DSSCs based on B and MB was evaluated under standard solar illumination (100 mW/cm^2). The DSSC sensitized with B exhibited a higher power conversion efficiency (PCE) of 0.31% and a short-circuit current density (J_{sc}) of 2.31 mA/cm^2, whereas the DSSC sensitized with MB demonstrated a lower efficiency (0.14%) and J_{sc} of 0.91 mA/cm^2. Despite this decrease in efficiency, a 100-hour stability test showed that DSSCs sensitized with MB retained approximately 73% of their initial efficiency, while those based on B retained only 31%, highlighting a significant improvement in long-term stability. EIS characterization of DSSC based on the two different sensitizers were made. These results suggest that MB-based DSSCs are more durable and potentially more competitive with inorganic-based solar cells. Overall, the findings highlight the trade-off between initial efficiency and long-term stability and provide valuable insights into the development of natural dye-based DSSCs with improved performance.

Keywords Dye-sensitized solar cells (DSSC) · Betalain · Modified betalain · Photovoltaic performance · Chemical modification · Stability test

1 Introduction

Energy usage in both the industrial and residential sectors is gradually rising, thereby necessitating the integration of sustainable and renewable energy sources. Among these, solar energy is particularly promising due to its abundance, cost-effectiveness, and inexhaustible nature [1]– [2]. Photovoltaic technologies, which can be classified based on device architecture or material composition, are engineered to harvest solar radiation and convert it into electrical energy [3].

✉ Benamar Cheknane
ocheknane@yahoo.fr

✉ Giuseppe Calogero
giuseppe.calogero@cnr.it

[1] Laboratory of Physical Chemistry of Interfaces of Materials Applied to the Environment, University of Blida 1, Ouled Yaïch, Algeria

[2] Laboratory of Natural Products Chemistry and biomolecules, University of Blida 1, Ouled Yaïch, Algeria

[3] Dipartimento di Scienze Chimiche, Biologiche, Farmaceutiche e Ambientali, Università degli Studi di Messina, Messina, Italy

[4] Institute for Chemical and Physical Processes (IPCF)-National Research Council - Messina, Viale Ferdinando Stagno D'Alcontres, N. 37, 98158 Messina, Italy

[5] Istituto di Tecnologie Avanzate per l'Energia "Nicola Giordano" (ITAE), Salita S. Lucia sopra Contesse n. 5, 98126 Messina, Italy

This imperative has driven scientists to explore advanced photovoltaic technologies, including dye-sensitized solar cells (DSSCs) [4], a leading class of third-generation photovoltaic devices [3]. Since the pioneering photovoltaic system developed by O'Regan and Grätzel [5], DSSCs have attracted considerable attention owing to their simple fabrication process, environmental friendliness, low production cost, and promising performance [6]. A typical DSSC consists of a porous semiconductor layer (usually TiO_2 or ZnO), a dye sensitizer, an electrolyte (commonly I^-/I_3^-), and a counter electrode. The dye plays a central role by absorbing light and injecting electrons into the conduction band of the semiconductor. Ruthenium-based dyes have demonstrated excellent efficiencies (up to 12%), but their high cost and environmental concerns have prompted the search for natural alternatives. To address this, ongoing research efforts aim to enhance the optical and anchoring properties of natural dyes to improve overall device performance [7]. Natural pigments such as chlorophylls, carotenoids, anthocyanins, flavonoids, indigo, and betalains have all been investigated for their contributions to photoconversion in DSSCs [8]. Among these, betalains stand out due to their distinctive chemical structure and ease of extraction from sources such as red beet, *Amaranthus*, red turnip, or *Bougainvillea*. Betalains are broadly classified into two groups: red betacyanins, which absorb around 535 nm due to the association of various amino acids and amines with betalamic acid, and yellow betaxanthins, which absorb near 480 nm, resulting from the conjugation of betalamic acid with cyclodihydroxyphenylalanine. Several studies have reported that DSSCs using betalains as sensitizers can achieve photoelectric conversion efficiencies up to 1.7% [9]. In 2012, Calogero et al. compared various natural pigments and identified Sicilian prickly pear betalain as the most efficient, reaching a PCE of 2.06%. The study also examined the influence of pH and co-adsorbents on dye–semiconductor interactions, confirming the potential of chemically optimized betalains for DSSC applications [10]. In 2015, Calogero et al. published a comprehensive review on vegetable-based dyes in DSSCs, including betalains. The paper discussed performance limits, dye degradation pathways, and synthetic strategies to improve stability and electron injection. It also presented a roadmap for bio-inspired photovoltaic technologies and discussed economic considerations regarding natural vs. synthetic dyes [11]. More recently, in 2022, Barichello et al. investigated plasmon-enhanced DSSCs using gold nanoparticles embedded in TiO_2 and betalain from Sicilian prickly pear. This system exhibited doubled efficiency under full sunlight and reached 15% under indoor LED light, demonstrating the feasibility of natural dyes in indoor photovoltaics. A betalain-sensitized module was also fabricated, confirming its scalability [12]. Despite their promise, DSSCs still face limitations in efficiency and long-term stability. Researchers have explored several strategies to address these issues, including redox couple optimization [13], improved dye anchoring [14], advanced counter electrodes [15], and bandgap engineering of semiconductors used as photoanodes [16]. However, natural dyes generally suffer from degradation when exposed to light, temperature variations, and humidity. In this context, the present study focuses on the extraction of betalains from purple *Bougainvillea*, followed by a comparative analysis of pure betacyanin (B) and chemically modified betacyanin (MB) as photosensitizers (Fig. 1a, c). In purple *Bougainvillea*, the predominant pigment is betacyanin, while betaxanthin (Fig. 1b) is more common in red-orange varieties. For this reason, purple *Bougainvillea* was selected [17]. Chemical modification of betacyanin was carried out via a Minisci reaction [18], introducing new functional groups aimed at improving adsorption on TiO_2 and enhancing long-term dye stability.

2 Experimental

2.1 Extraction of betacyanin

Fresh purple *Bougainvillea* flowers were collected in southern Italy, particularly in Messina. To prepare the extract, 12

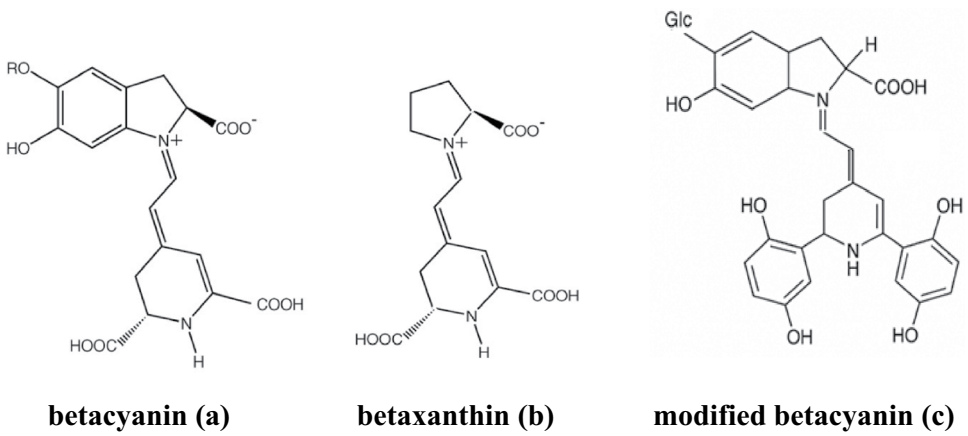

Fig. 1 Chemical structure of betacyanin (**a**), betaxanthin (**b**) and modified betacyanin (**c**)

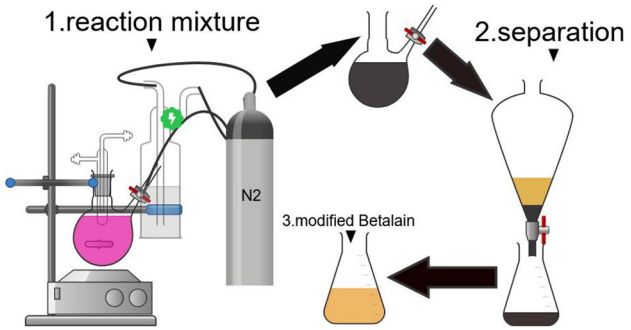

Fig. 2 A schematic illustration of the synthesis process for the chemical modification of betalain. Step 1: The reaction components were introduced into a flask, subjected to purging, and maintained under a nitrogen atmosphere with continuous stirring for 24 h. Step 2: The organic layer was extracted using ethyl acetate. Step 3: The modified betalain was then filtered and concentrated

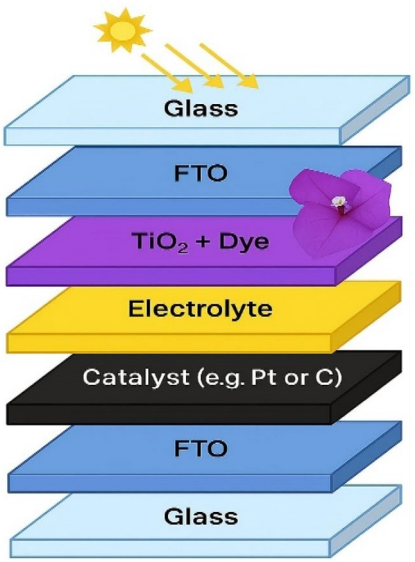

Fig. 3 Structure of dye-sensitized solar cell (DSSC)

g of dried flowers were ground in 500 milliliters of acidic water with a pH of 3. This mixture was stabilized by adding 0.2% citric acid and 0.1% ascorbic acid. After filtering the mixture, the residue was further macerated until the powder color disappeared. Betacyanin content was measured using UV-Vis spectroscopy [19].

2.2 Synthesis of the modified betacyanin

The extraction yield was approximately 8.75%. The crude extract contained not only betacyanin but also other natural compounds such as phenols [20]. However, the amount of pigment obtained was relatively small, and its purification would require several chromatographic steps, making the process both complex and expensive. Therefore, it was more practical to use the crude extract directly in subsequent reactions. In this context, the crude purple dye extract was used without further purification.

The following ingredients were added to a vacuum flask: 0.2 mmol quinone, 0.4 mmol purple dye, 1 mL ethanol, and 0.9 mL water. Next, silver nitrate ($AgNO_3$ 0.1 ml of 0.4 M, 0.4 mmol) and 0.4 mmol of ammonium persulfate ($(NH_4)_2S_2O_8$, 91 mg) were added all at once (Figs. 2 and 3). The flask was purged and kept under a nitrogen atmosphere before being securely sealed with a screw cap. The mixture was stirred at room temperature for 24 h. After completion, the aqueous phase was extracted with ethyl acetate. The organic solvent was dried over magnesium sulfate, then filtered and concentrated by rotavapor (Fig. 2). The raw substance acquired was dissolved in deuterated methanol for NMR yield assessment [18].

2.3 Device fabrication and characterization

The FTO-glass substrates, measuring 15 cm × 4 cm, were washed in a detergent solution, rinsed with a water/ethanol mixture, and then dried in an oven set at 80 °C. Next, the FTO conducting glass plates were treated with TiO_2 nanocrystalline layers via screen printing using polyester mesh with a 43/80 specification (43 thread per inch, 80-micron thread diameter) mesh. The process involved coating the plates, storing them in ethanol, and drying them at 125 °C. This process was repeated multiple times, depending on the desired TiO_2 film thickness, afterward, the plates were sintered at 500 °C for 30 min, followed by cooling down to room temperature.

Depending on the number of TiO_2 layers deposited, the resultant transparent mesoscopic oxide films were approximately 14 µm thick after sintering (as determined using a BRUKER DektakXT profilometer). The total surface area of each spot was 0.181 cm^2. After determining the dimensions of the TiO_2 film, the plates that had been screen-printed and cooled were cut into rectangular shapes with dimensions of 2 cm × 1.5 cm. These plates were then immersed in a solution of betalain dye and modified betalain (MB) overnight at room temperature in the dark. To get rid of the excess dye, the photoanodes were washed using the same solvent that was used in the dye solution then dried in an oven at a temperature of 80 °C for a brief time. A thin and transparent TiO_2 film was produced using the doctor-blade process to be used as the photoanode for UV-Vis absorption measurements (Jasco V-730 UV–Vis Spectrophotometer). To prepare the counter-electrode, a 1.0 mm diameter hole was drilled into a FTO glass plate (2 cm x 1.5 cm). After the perforated substrates were thoroughly rinsed with water and ethanol, all remaining organic contaminants and glass debris were removed. The conductive side of the FTO glass was treated with a transparent platinum catalyst (PT1,

Greatcell Solar) using the doctor-blade method. To ensure uniform film thickness and preserve an electrical contact area, one edge of the plate was covered with a strip of adhesive tape (3 M Magic). The platinum paste was uniformly applied to the substrate by gliding a glass rod over the tape spacer mask. After the removal of the adhesive tape, the glass plates were heated at 550 °C for one hour. The photoanode and the platinum counter-electrode were assembled in a sandwich-like structure (Fig. 3) and sealed with a thermopress with a Surlyn ionomer gasket (Meltonix 1170-25, Solaronix SA). The electrolyte containing the I^-/I_3^- redox couple was injected into the cell vacuum backfilled through a hole in the back of the cathode. The hole was then securely sealed with adhesive tape and resulting DSSC (Fig. 4) was electrically contacted by metal solder [10].

The current–voltage curves were recorded using a computer-connected Keithley SourceMeter (Model PVIV-1 A) to conduct photoelectrochemical measurements. An Oriel solar simulator (Model LCS-100 Small Area Sol1A) was used to simulate sunlight irradiation. This simulator was equipped with a 300 W Xe Arc lamp and an AM 1.5 filter, providing a light intensity of 100 mW/cm^2. The maximum output power (P_{max}) was obtained from the I-V characteristics curve at the point where the product of voltage and the corresponding current was at its peak. P_{max} (Eq. (1)) was evaluated using the following equation:

$$P_{max} = V_{max} \times J_{max} \tag{1}$$

FF determined the overall performance of the cell. The FF (Eq. (2)) and efficiency of the cell, η (Eq. (3)) has been determined by using the following relations [10].

$$FF = \frac{Pmax}{Jsc \times Voc} \tag{2}$$

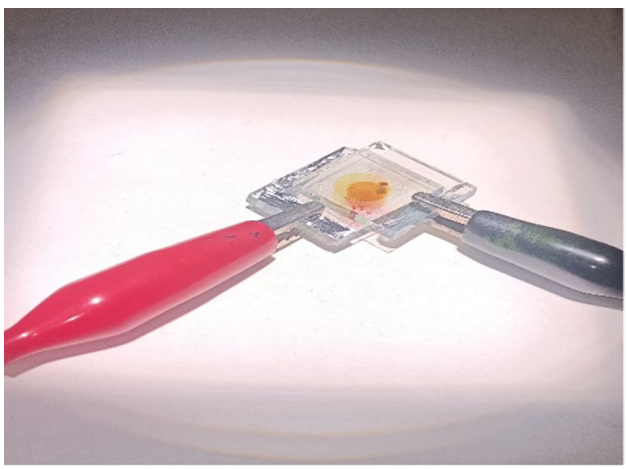

Fig. 4 DSSC contacted and assembled

With J_{sc} and V_{oc} were the short circuit current density and the open circuit voltage.

$$\eta = \frac{J_{sc} \times V_{oc} \times FF}{Pin}, \tag{3}$$

where P_{in} is the input power (100 mW/cm^2).

The IPCE (or Incident photon to current efficiency) is the fraction of incident monochromatic photons that are converted into collected electrons at a given wavelength; it quantifies the device's wavelength-resolved photoconversion. The IPCE was measured under monochromatic illumination (300–800 nm) using a monochromator and a **Solarena** calibrated radiometric reference.

It is calculated according to Eq. (3b) as :

$$IPCE = \frac{1.24 \times J\ (\mu A\,cm^{-2})}{\lambda\,(nm) \times P\lambda\ (mW\,cm^{-2})} \tag{3b}$$

where $P\lambda$ is the incident power of the monochromatic wavelength measured with a referenced Si cell.

To quantify the amount of dye adsorbed onto the TiO_2 surface, we followed the solution depletion/film absorbance method described by Zhang et al. [21] for betalain-sensitized TiO_2 photoelectrodes. The experimental procedure was performed as follows:

1. A 3.00 mL aliquot of the dye bath (0.60 mM) was recorded by UV–Vis before and after immersing a 1 cm^2 TiO_2 film (14 µm thick).
2. The decrease in peak absorbance (ΔA_{535} for B; ΔA_{500} for MB) was converted to a concentration change (Δc) using $\varepsilon = 6.5 \times 10^4\ M^{-1}\ cm^{-1}$ for betalains.

$$\text{Mole uptake} = \Delta c \cdot V \text{ and the surface coverage } \Lambda = \text{moles/area}$$

Furthermore, the DSSCs were tested with an Autolab potentiostat/galvanostat (Metrohm) equipped with a frequency-response analyzer. Electrochemical impedance spectroscopy (EIS) was carried out from 100 kHz to 0.1 Hz at 0.2 V under illumination, using a 10 mV_rms sinusoidal perturbation. The impedance spectra were fitted in NOVA software (Metrohm) with an equivalent circuit consisting of a series resistance (Rs) in series with two parallel Voigt elements (Rp1||CPE1 and Rp2||CPE2), which capture two distinct relaxation processes attributed to interfacial charge transfer at the counter-electrode/electrolyte and photoanode/electrolyte interfaces, respectively.

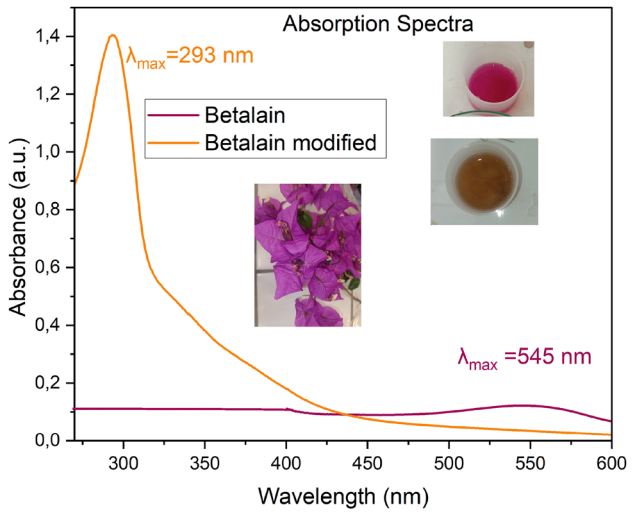

Fig. 5 UV–Vis absorption spectra of natural (B) extracted from Purple *Bougainvillea* and MB

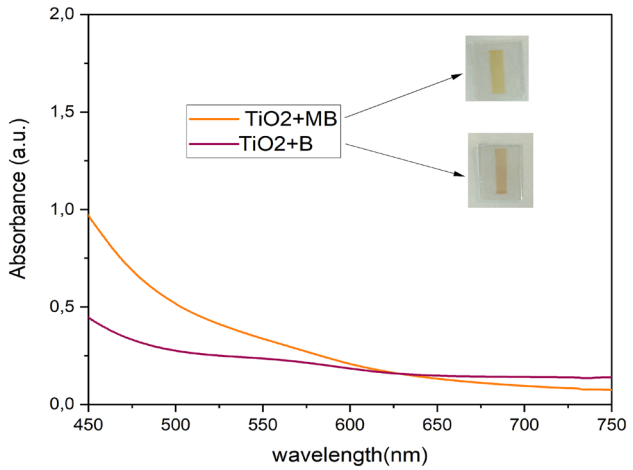

Fig. 6 Absorption spectra of photoanodes sensitized with (B) and (MB)

3 Results and discussions

3.1 Absorption spectra

The UV–Vis absorption spectrum in arbitrary unit (a.u.) of the Purple *Bougainvillea* extract, diluted in deionized water, was analyzed. Figure 5 shows a significant difference between the absorption spectra of natural betalain (B) and chemically MB. Before modification, betalain exhibited weak absorption in the visible region, with a peak at 545 nm, corresponding to its characteristic red-violet betacyanin group. After chemical modification, a strong absorption band appeared in the ultraviolet region, with a prominent peak at 293 nm. This spectral shift is similar to that reported for anthocyanins when modified by pH changes or by interaction with TiO_2 through hydroquinone groups [11]. In the case of betalains this behavior suggests a change in the electronic transitions of the chromophore, likely due to the introduction of new functional groups that alter their light absorption properties.

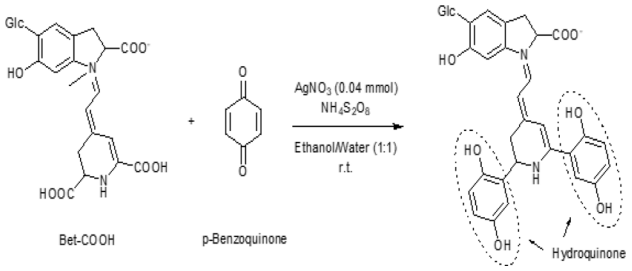

Fig. 7 Reaction scheme of betalain modification

The absorbance spectrum of electrodes sensitized with betalain (TiO_2+B) and MB (TiO_2+MB) reveals a clear enhancement in absorption following chemical modification. As shown in Fig. 6, the absorbance of the (TiO_2+MB) photoanode is higher than that of (TiO_2+B), indicating a higher optical density of TiO_2+MB compared to TiO_2+B. This increase is consistent with the higher dye loading of MB (Table 1) and its higher LHE; however, the lower J_{sc} of MB suggests that electron injection (rather than absorption) is the primary limitation.

3.2 Mechanism for the chemical modification by radical decarboxylation of betalain

In this reaction (Fig. 7), silver nitrate ($AgNO_3$) is activated in the presence of ammonium persulfate ($(NH_4)_2S_2O_8$), which acts as a strong oxidizing agent. The persulfate is first reduced to generate sulfate radicals ($SO_4^{-\cdot}$) capable of oxidizing silver(I) ions to silver (II). The resulting Ag^{2+} ions can then oxidize carboxylated betalain (Bet-COOH), leading to the formation of a carboxyl radical (Bet-COO$^{\cdot}$). This unstable intermediate undergoes spontaneous decarboxylation with the release of carbon dioxide, producing a free radical centered on the aromatic ring of the betalain (Bet$^{\cdot}$). This radical subsequently reacts by addition to the conjugated ring system of p-benzoquinone, resulting in the formation of a stable coupling product of the hydroquinone type. This mechanism highlights an oxidative radical

Table 1 Photovoltaic characteristics of the fabricated DSSC

Dye	J_{sc}	V_{oc}	FF	η %	ΔA	Γ (μmol cm^{-2})	Γ_mass (μg cm^{-2})
B (n=3)	2.31±0.15	0.35±0.03	0.38±0.03	0.31±0.02	0.118	0.061	23
MB (n=3)	0.91±0.12	0.29±0.05	0.49±0.01	0.14±0.01	0.226	0.117	41

transformation that enables the functionalization of betalain through aromatic coupling with benzoquinone (Fig. 8).

The reaction yielded 0.73 g of MB from an initial 1.05 g of crude betalain extract, corresponding to a yield of approximately 69.5%.

3.3 Fourier transform infrared spectroscopy and nuclear magnetic resonance (NMR) spectroscopy

The FTIR analysis confirms significant structural modifications in betalain following chemical treatment, highlighting the introduction of new functional groups relevant to its improved performance in DSSCs. Figure 9 shows a comparison between B and MB, revealing key differences in functional group composition that may influence their interaction with TiO_2 and the electrolyte. The region around 3300 cm^{-1} indicates the presence of hydroxyl (–OH) groups, particularly phenolic ones, consistent with betalain and hydroquinone structures. This broad band may also involve N–H stretching vibrations, as betalains contain nitrogen atoms; its width likely results from hydrogen bonding interactions [22]. A noticeable shift and weakening of the carbonyl (C=O) stretching band near 1644 cm^{-1}, associated with carboxylic acids or newly formed ester or amide linkages, suggests structural reorganization as a result of chemical modification, possibly involving hydroquinone. This band may also partially correspond to conjugated C=C bonds. Both carbonyl and hydroxyl groups are crucial for anchoring dyes to TiO_2 photoanodes, making them valuable functional motifs for efficient electron injection in DSSCs [23, 24]. The appearance of new bands between 1300 and 1000 cm^{-1}, attributed to C–O stretching vibrations, confirms the presence of ether and ester groups. These functionalities can enhance dye solubility, promote interaction with the electrolyte, and improve chemical stability. Modifications in the π-conjugated system, induced by the chemical treatment, appear to reduce the effective conjugation length, leading to a blue shift in the absorption spectrum. This is evidenced by the appearance of a strong UV band at 293 nm in MB, which suggests altered electron delocalization and modified HOMO–LUMO transitions. Finally, the changes observed below 900 cm^{-1}, attributed to C–H bending modes of alkene groups, further support the hypothesis of rearranged structural motifs that could impact both light absorption and dye anchoring behaviour. These results confirm that the chemical modification not only alters existing functional groups but also introduces new ones (e.g., esters, ethers, conjugated structures), optimizing dye adsorption onto TiO_2, enhancing interfacial charge transfer, and increasing dye stability within the DSSC system (Fig. 9).

The FTIR spectrum (Fig. 9) show several key absorption bands that support the structural characteristics identified

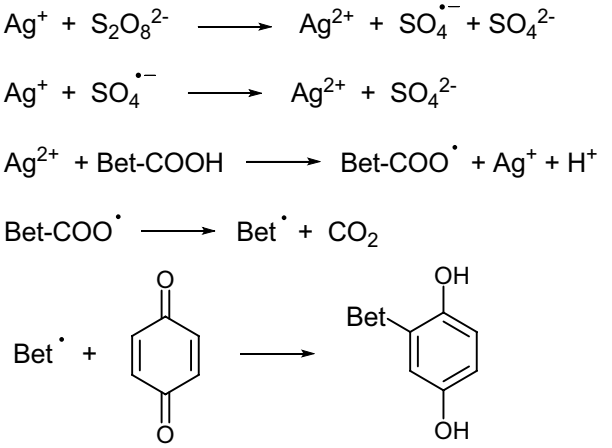

Fig. 8 The suggested mechanism for the chemical modification of betalain by Minisci reaction

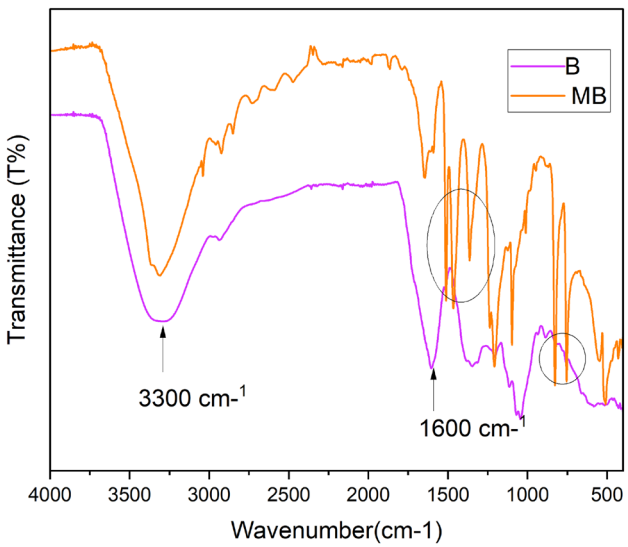

Fig. 9 FTIR spectra of betalain (B) and modified betalain (MB): structural changes and functional group analysis

in the ^1H NMR analysis (Fig. 10). The strong O–H stretch around 3300 cm^{-1} in the FTIR spectrum indicates the presence of hydroxyl and phenolic groups, consistent with signals expected in the 4–12 ppm range in the ^1H NMR, which are exchangeable with deuterium from the CD_3OD solvent. These correspond to the –OH protons of betalains and the phenolic –OH groups of the hydroquinone moiety, with their exact chemical shifts influenced by their environment and hydrogen bonding. Additionally, the C=C stretching at approximately 1611 cm^{-1} and the C–H bending below 900 cm^{-1} confirm the presence of aromatic rings, aligning with the 6.0–8.5 ppm region. The introduction of a hydroquinone group would be expected to enhance or modify the signal pattern in this aromatic region. Furthermore, the C=O stretching band around 1644 cm^{-1} suggests the presence of carbonyl functionalities, indicating possible ester

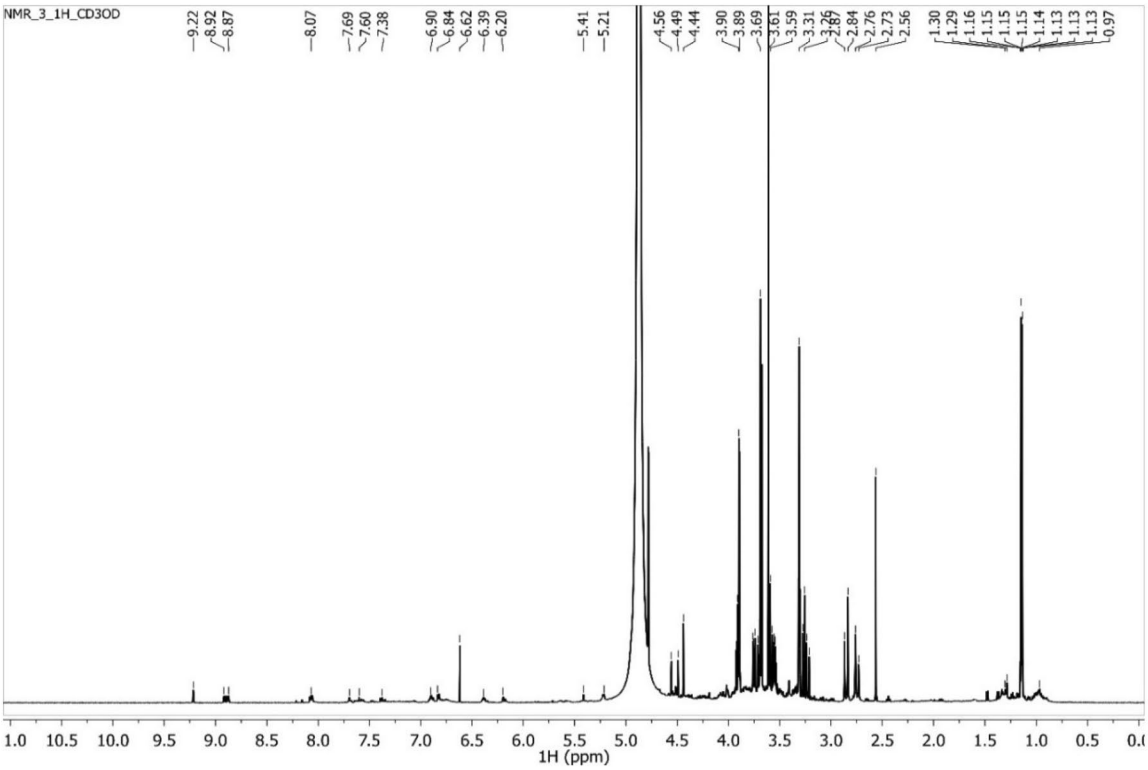

(a)

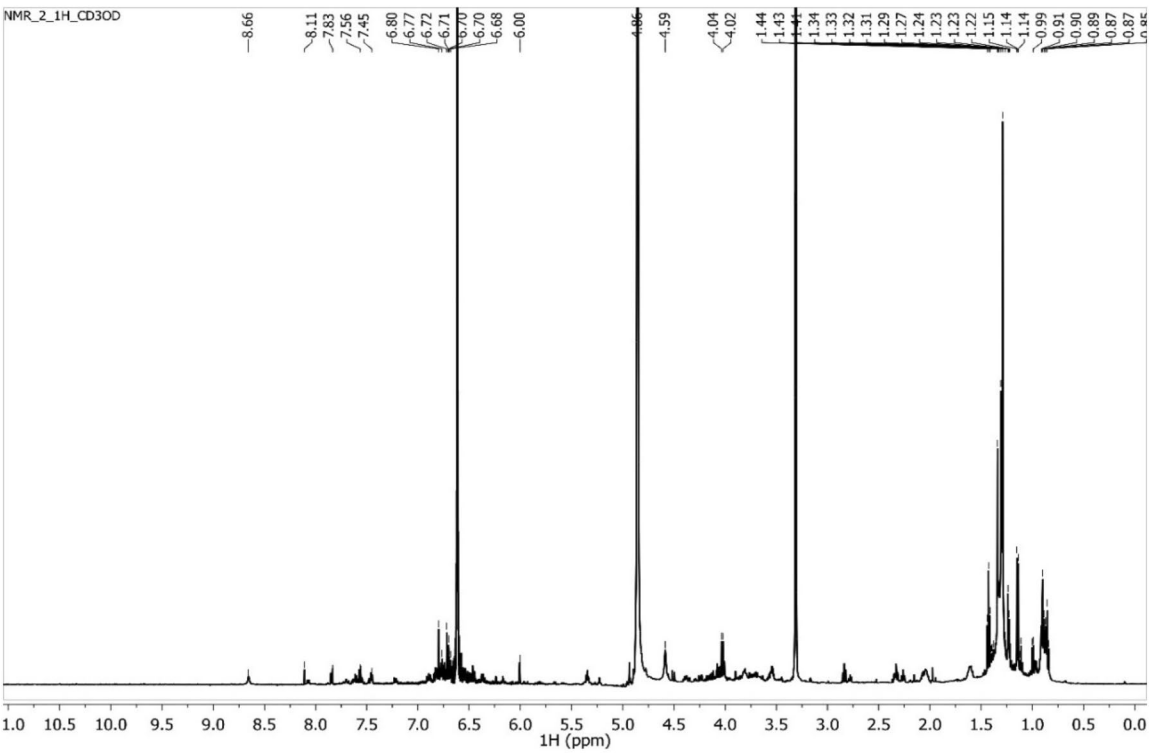

(b)

Fig. 10 ^{1}H NMR spectrum of betanin (**a**) modified betalain (**b**)

or amide formation during the modification. Such changes could affect the chemical shifts of protons adjacent to the new carbonyl groups, such as –CH_2–O–CO– or –CH_2–NH–CO– environments. Finally, multiple peaks between 1300 and 1000 cm^{-1} in the FTIR spectrum highlight the presence of C–O bonds, supporting the existence of alcohol, phenol, and potentially ether or ester linkages, which correspond to proton signals typically observed in the 3.5–5.5 ppm range in the ^{1}H NMR spectrum.

3.4 Photoelectrochemical properties

Dye-sensitized solar cells (DSSCs) based on natural dyes such as betalains have demonstrated substantial potential due to their environmental sustainability and low production cost [10–12]. Here we compare the electrical behavior of DSSCs sensitized with unmodified betalains (B) and chemically MBs, with particular attention to the estimation of the series resistance (R_s) and the shunt resistance (R_{sh}) derived from experimental IV curves and corresponding tabulated data. Figure 11 shows the J-V curves of the assembled DSSC using B and MB measured at 100 mW/cm^2 under solar simulator. All the photovoltaic parameters are listed in Table 1.

The results show that the DSSC sensitized with (B) exhibits a higher J_{sc} (2.31 mA/cm^2) and efficiency (0.31%) compared to the DSSC based on (MB), which has a lower J_{sc} (0.91 mA/cm^2) and η (0.14%). This decrease in Jsc for MB may be attributed to less effective dye adsorption on the TiO_2 surface or altered electron transfer dynamics after chemical modification. Additionally, it can be explained by the fact that high adsorption may lead to dye aggregation, thereby reducing the active surface area available for charge transfer.

Compared to other natural dye-based DSSCs, the performance achieved with B (η = 0.31%) is consistent with devices sensitized using unmodified plant-derived dyes.

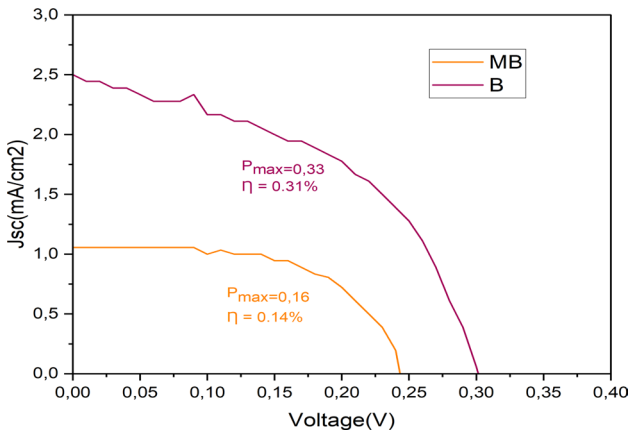

Fig. 11 Current voltage for B and MB solar cells

For instance, Erande et al. reported an efficiency of 0.2% for DSSCs using anthocyanins extracted from pomegranate juice [25]. Yazie et al. achieved 0.175% for a quasi-solid-state DSSC employing pigments from *Bougainvillea spectabilis* extracted in acidified ethanol [26]. Hemalatha et al. reported efficiencies of 0.29% and 0.22% using anthocyanins and carotenoids extracted from *Rosa chinensis* and *Kerria japonica*, respectively [27]. On the other hand, the results obtained for MB are in line with those reported by Martinez et al. [17], who found that the short-circuit current (Jsc) was lower when using MB compared to without modification.

The current voltage behaviour of a solar cell, including the effects of R_s and R_{sh}, is described by:

$$J(V) = J_{\mathrm{ph}} - \mathrm{J}_0 \times \left[e^{\left(\frac{q(V+J\cdot \mathrm{Rs})}{(\mathrm{n}\cdot \mathrm{k}\cdot \mathrm{T}}\right)} - 1\right] - \frac{(\mathrm{V} + \mathrm{J}\cdot \mathrm{R_s})}{R_{sh}} \quad (4)$$

At short-circuit conditions (V = 0):

$$J_{\mathrm{sc}} = J_{\mathrm{ph}} - \mathrm{J}_0 \times \left[e^{\left(\frac{q\cdot \mathrm{Jsc}\cdot \mathrm{Rs}}{(\mathrm{n}\cdot \mathrm{k}\cdot \mathrm{T}}\right)} - 1\right] - \frac{(\mathrm{Jsc}\cdot \mathrm{Rs})}{R_{sh}} \quad (5)$$

For $R_s \approx 0$ and $R_{sh} \to \infty$, the approximation is:

$$J_{\mathrm{sc}} \approx J\mathrm{ph}$$

The current density J is defined as I normalized to the active area (mA/cm^2). To estimate R_s and R_{sh}, the initial and final slopes of the experimental IV curves are used. The following relationships apply:

- Series Resistance (R_s): This is estimated from the slope at the high-voltage end of the IV curve (near V_{oc}).
- Shunt Resistance (R_{sh}): This is estimated from the initial slope of the IV curve (near V = 0).

We approximate Calculations (R_{sh} and R_s estimation) from IV Curves for both the DSSC with betalain (B) and with MB: our results were reported in Table 2.

The differences in R_s and R_{sh} values reflect the distinct characteristics of the IV curves: The B cell shows higher short-circuit current but a more rounded IV curve (low R_s, low R_{sh}). The MB cell exhibits a higher fill factor, more rectangular IV curve and higher R_{sh}, indicating improved charge separation and longer-term stability. In the case of the MB cell, the estimated R_s is higher (~ 150 Ω cm^2) than in the B cell (~ 100 Ω cm^2), leading to increased ohmic losses and consequently a lower J_{sc} (0.91 mA/cm^2 vs. 2.31 mA/cm^2). At the same time, the higher R_{sh} observed in the MB device (~ 30 Ω cm^2 vs. ~ 21.7 Ω cm^2) implies superior suppression of leakage currents and improved diode behaviour,

Table 2 Rs and R_{sh} Estimation for DSSC based on betalain (B) and modified betalain (MB)

Dye	R_s (Ω cm^2)	R_{sh} (Ω cm^2)
B	~100	~21.7
MB	~150	~30

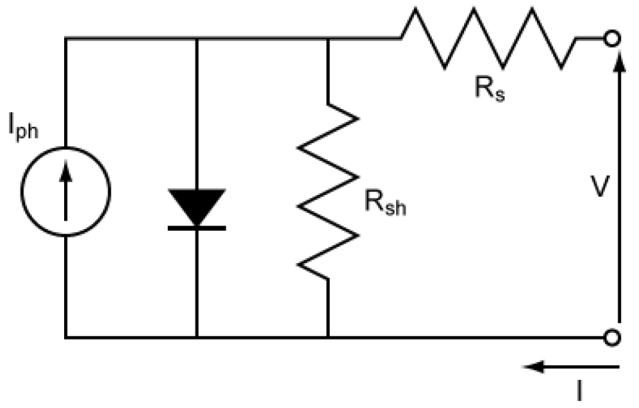

Fig. 12 Equivalent circuit of a dye-sensitized solar cell (DSSC), where I is the output current flowing through the external load. The model includes a photocurrent source (I_{ph}), a diode (recombination), a shunt resistance (R_{sh}), and a series resistance (R_s)

which is consistent with the more rectangular IV curve and higher fill factor (0.49 for MB vs. 0.41 for B). These findings affirm that although the chemical modification improves interfacial stability and reduces parasitic recombination (via increased R_{sh}), it may also introduce structural or electronic barriers that hinder charge injection or transport (reflected by increased R_s). The trade-off is a lower J_{sc} but enhanced long-term operational stability and voltage retention. Such insights underline the importance of concurrently optimising R_s and R_{sh} to maximise overall power conversion efficiency (PCE). The observed differences between B and MB can be attributed to chemical modifications. The replacement of the carboxylic group with a hydroquinone moiety (in MB) enhances anchoring on TiO_2 and stabilises the dye. However, this modification may reduce the electron injection rate, consistent with the lower J_{sc}. Future studies should measure injection kinetics directly using techniques such as transient absorption spectroscopy.

Figure 12 illustrates the one-diode equivalent circuit model of a dye-sensitized solar cell (DSSC), which is widely used to describe its electrical behaviour. The schematic includes the following key components:

- A photocurrent source labelled I_{ph} representing the current generated by photoexcited electrons injected into the TiO_2 conduction band from the dye molecules upon illumination.
- A diode placed in parallel with the photocurrent source, modelling the recombination of electrons with the oxidized species in the electrolyte (typically the redox couple).
- A shunt resistance R_{sh}, also in parallel, representing leakage pathways or non-ideal recombination routes through the cell.
- A series resistance R_s, connected between the internal circuit and the external terminals, accounting for resistive losses due to the transparent conducting oxide (TCO), the electrolyte, and the interfaces within the cell.
- The voltage V across the terminals and the current III flowing through the external load are also indicated.

In the context of DSSCs, the output current density J used previous is defined as the current I normalised over the active area of the photoanode and is typically expressed in milliamperes per square centimetre (mA/cm^2). This normalisation is essential for comparing the photovoltaic performance of DSSCs of different geometries.

The following graph (Fig. 13) displays the estimated R_s and R_{sh} values for the two DSSC devices:

The comparative bar chart (Fig. 13) visually reinforces the numerical analysis by clearly illustrating the differences in internal resistances between the two DSSC configurations. The MB device exhibits a noticeably higher series resistance (R_s), which aligns with its reduced short-circuit current density, as predicted by the current–voltage equation. Simultaneously, its higher shunt resistance (R_{sh}) is indicative of better suppression of leakage currents and a more ideal diode behaviour. In contrast, the unmodified betalain (B) cell displays lower R_s and R_{sh} values, which contribute to a higher J_{sc} but a lower fill factor. This visual representation succinctly encapsulates the inherent trade-off between charge transport efficiency and device stability in these natural dye-based photovoltaic systems. We also performed IPCE measurements for TiO_2|B and TiO_2|MB (not reported because of low values obtained) in fact the action spectra show a maximum in the green region (~560 nm), with low peak values (~2–3%), consistent with "green" devices lacking $TiCl_4$ post-treatment and co-adsorbents. Absolute IPCE values are intrinsically lower when (i) TiO_2 electrodes are not treated with $TiCl_4$ and (ii) natural dyes (extracts/derivatives) are used, compared with synthetic dyes and optimized electrode protocols. $TiCl_4$ post-treatment is known to improve the TiO_2 microstructure (increased active surface area, reduced trap density, improved substrate contact), thereby increasing J_{sc}/IPCE; our 'green' choice deliberately avoided such passivation.

3.5 Stability test

Besides photoelectrochemical stability, in our previous work [9] thermal stability was evaluated by calorimetric

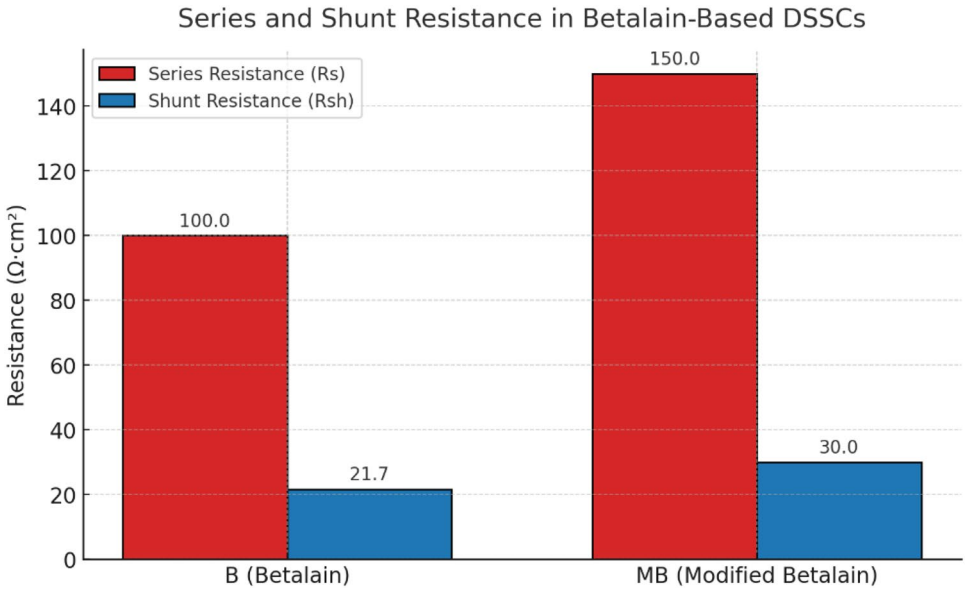

Fig. 13 Graph displaying estimated series and shunt resistance for betalain and modified betalain based DSSC

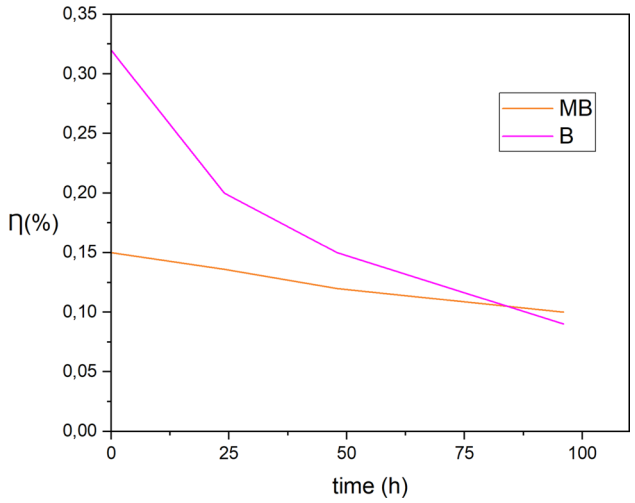

Fig. 14 Evolution of the efficiency of DSSCs sensitized with B and MB over time

analysis. The result demonstrated thermal stability below 160 °C and a decomposition process starting at 180 °C. These results indicate that betalain dyes (adsorbed in TiO_2 matrix) are thermally stable at the temperatures reached by the operational cell under solar irradiation. In this work a stability test was conducted on the solar cells sensitized with B and MB. As shown in Fig. 14, the initial power conversion efficiency of the DSSC based on B is approximately 0.31%, but it decreases significantly to around 0.10% after 100 h of operation representing a loss of nearly 69%. In contrast, the DSSC based on MB starts with a lower initial efficiency of about 0.14%, yet it decreases more gradually to approximately 0.11%, corresponding to a loss of around 27%. This slower degradation observed with MB indicates better stability over time. Therefore, while the chemical modification applied in MB does not improve the initial photovoltaic performance, it contributes to a more stable device. These findings suggest that further optimizing the modification strategy could enhance the long-term stability of DSSCs while minimizing the initial performance loss.

3.6 EIS characterization

Electrochemical impedance spectra of the DSSCs (Fig. 15) exhibit two well-resolved semicircles under illumination at 0.2 V, which are accurately described by an equivalent circuit composed of a series resistance (R_s) and two parallel Voigt elements (Rp1‖CPE1 and Rp2‖CPE2) (inset of Fig. 16). This topology captures two dominant relaxation processes in operative dye-sensitized cells: a high-to-mid-frequency response (Rp1‖CPE1), commonly associated with the charge-transfer reaction at the counter-electrode/electrolyte interface and its interfacial double-layer/dispersion, and a mid-to-low-frequency response (Rp2‖CPE2), largely governed by recombination/transport at the photoanode/electrolyte interface together with the chemical (accumulation) capacitance of the mesoporous oxide under illumination. Use of constant-phase elements (CPEs) instead of ideal capacitors accounts for interfacial heterogeneity and non-Debye behavior expected in rough catalytic layers and porous photoanodes.

We built two cells with unmodified betalain (B1 and B2) and two with modified betalain (MB1 and MB2), the cells were fabricated in order to investigate their EIS performances.The excellent agreement between experimental and fitted points for all devices (B1, B2, MB1, MB2), plotted as “data” vs. “fitting” in the Nyquist diagram, indicates that diffusion contributions are minor in the probed window, as the spectra close toward the real axis without a

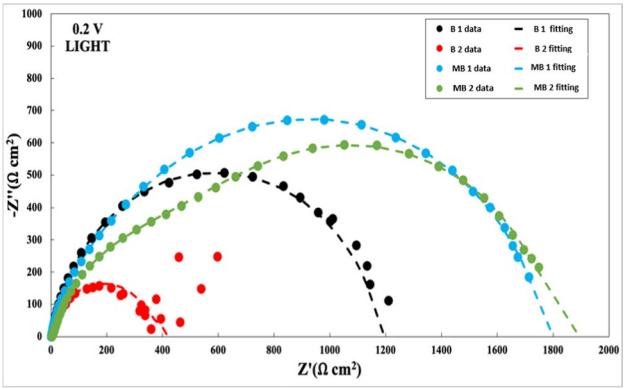

Fig. 15 Nyquist plots at 0.2 V under illumination (10 mV_rms, 100 kHz–0.1 Hz): symbols are data and dashed lines NOVA fits to Rs–(Rp1‖CPE1)–(Rp2‖CPE2)

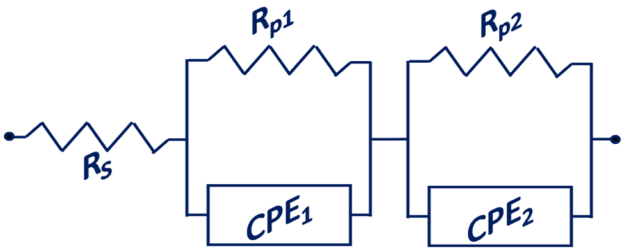

Fig. 16 Equivalent circuit used for EIS fitting: a series resistance (Rs) in series with two parallel branches (Rp1‖CPE1 and Rp2‖CPE2). *CPE* constant phase element

45° "Warburg tail." Consequently, adding a mass-transport element (finite-length Warburg) is unwarranted under these conditions. The fitted series resistance, Rs, represents the ohmic backbone of the cell—electrolyte resistance, FTO/TCO sheet resistance, wiring, and contact losses.

Although the absolute values are reported in Table 3, qualitative trends are evident: the B2 device shows the left-most intercept and the smallest overall arc, indicating a lower Rs than B1 and the MB series. This points to improved current collection and/or higher electrolyte conductivity in B2, plausibly arising from better catalyst coverage/adhesion at the counter electrode, optimized redox concentration, or reduced contact resistance at the current collectors. By contrast, MB1 and MB2 present larger real-axis intercepts, consistent with additional ohmic drops e.g., thicker catalytic over-layers, less conductive binders, or slightly higher TCO sheet resistance after processing. Beyond ohmic losses, the arc sizes reveal the hierarchy of interfacial kinetics. The smallest semicircles of B2 across the entire frequency span indicate the lowest interfacial impedances; both Rp1 and Rp2 are reduced compared to B1, implying (i) faster charge transfer at the counter electrode (lower Rp1) and (ii) suppressed recombination or enhanced electron transport at the photoanode (lower Rp2). In practical terms, B2 should sustain higher photocurrent at a given photovoltage, translating into improved fill factor under illumination. The MB devices display the opposite trend: MB1 exhibits the largest mid-to-low-frequency arc, signaling a substantial increase of Rp2 and thus slower interfacial charge extraction or higher recombination probability in the photoanode network. MB2 partially mitigates this effect (smaller arc than MB 1 but still larger than B1), suggesting that the modification improves one of the limiting steps likely either the catalytic activity at the counter electrode or the surface passivation of the photoanode yet does not fully recover the kinetic advantage observed for B2. The dispersive exponents of the CPEs (n1 and n2) provide a compact metric of interfacial uniformity ($n \rightarrow 1$ for an ideal capacitor). Values closer to unity imply narrower distributions of time constants and smoother, more homogeneous interfaces.

Although full parameter values are listed in Table 3, the fits consistently required $n < 1$ for both elements, corroborating the expected heterogeneity of porous electrodes. The MB series typically demanded lower n_2 than B1/B2 in order to reproduce the flattened low-frequency arcs, which we interpret as increased morphological/chemical disorder at the photoanode/electrolyte interface after modification. This conclusion is consistent with the larger R_{p2} found for MB 1/MB2 and suggests that further optimization should target surface passivation and pore-scale electrolyte wetting to recover a higher effective chemical capacitance with reduced dispersion. From a device-engineering standpoint, the comparative picture is clear: B2 represents the best-balanced configuration, combining low ohmic loss (small Rs), fast counter-electrode kinetics (low R_{p1}), and reduced recombination/efficient transport at the photoanode (low R_{p2} with moderate dispersion). B1 is a solid baseline but suffers from higher interfacial resistances, while MB1 despite the intended improvements introduces additional barriers at the photoanode side, as evidenced by its dominant low-frequency arc and stronger non-ideality (lower n_2). MB2

Table 3 Equivalent-circuit parameters extracted from EIS fitting at 0.2 V under illumination for samples B1, B2, MB1, and MB2 using the model Rs–(Rp1‖CPE1)–(Rp2‖CPE2) (parameters: Rs, Rp1, Rp2, Y1, n1, Y2, n2)

	Rs (Ω cm^2)	R_{P1} (Ω cm^2)	CPE_1		R_{p2} (Ω cm^2)	CPE_2	
			Y_1 (S s^N)	N_1		Y_2 (S s^N)	N_2
B1	12.7	230	0.15×10^{-3}	0.909	975	9.1×10^{-2}	0.344
B2	13.5	75	6×10^{-3}	0.954	335	7.29×10^{-5}	0.49
MB1	11.9	575	2×10^{-4}	0.914	1239	1.2×10^{-4}	0.857
MB2	14.3	437	1.8×10^{-4}	0.877	1534	6.5×10^{-5}	0.817

partially corrects these penalties but does not yet match B2. These insights suggest two immediate optimization levers for the MB path: (i) restoring/boosting counter-electrode activity (e.g., catalyst loading, annealing, binder/ionomer selection) to reduce R_{p1} without increasing Rs, and (ii) surface passivation or co-adsorbent strategies at the photoanode to lower R_{p2} and raise n_2, thereby sharpening the low-frequency response. In summary, the dual-Voigt equivalent circuit provides a compact yet discriminating fingerprint of illuminated DSSC operation at 0.2 V. Combined with t the Nyquist overlays, it reveals that improvements in B2 are systemic ohmic, catalytic, and photoanode interfacial whereas the MB series exhibits trade-offs centered on the photoanode interface. The extracted parameters (Rs, Rp1, Rp2, Q1, n1, Q2, n2) reported in Table 3 will be used below to quantify how these kinetic signatures propagate to J–V metrics and to rationalize device-level performance under continuous illumination.

4 Conclusion

The performance and long-term reliability of dye-sensitized solar cells (DSSCs) are significantly constrained by the intrinsic photochemical instability of natural dyes, which tend to degrade rapidly under environmental stressors, including prolonged light exposure, thermal fluctuations, and humidity. This fundamental limitation has stimulated extensive research aimed at improving dye stability through various approaches, such as structural modifications via chemical reactions, the incorporation of molecular stabilizers, and the optimization of dye extraction protocols. In this context, our study explored the chemical functionalization of betalain pigments derived from *Bougainvillea glabra* via a Minisci-type radical substitution approach. This strategy facilitated the introduction of specific functional groups that increased the affinity of the dye molecules for TiO_2 surfaces, thus enhancing their anchoring capability and interaction with the semiconductor. Experimental comparison between unmodified betalain (B) and the chemically modified derivative (MB) revealed a nuanced trade-off between photovoltaic efficiency and long-term stability. While B-sensitized DSSCs exhibited superior initial power conversion efficiency (PCE), the MB-based devices demonstrated significantly improved operational stability over extended periods. This behaviour is consistent with EIS analysis of MB2, which exhibits a larger MF–LF arc (higher R_{p2}) and a higher $R_s$than B2, pointing to greater ohmic losses and an electronic bottleneck at the photoanode (recombination/transport) that prevents the increased LHE from translating into usable current. Consequently, despite the higher stability of the modified dye, B2 remains more efficient (higher $J_{sc}$and FF) than MB2.These findings suggest that targeted chemical modification, while potentially sacrificing some degree of short-term performance, plays a crucial role in extending the functional lifespan of natural dye-sensitized systems. Such a trade-off points to the need for further optimization of the chemical tailoring process, with a particular emphasis on achieving synergistic effects between light-harvesting capacity and structural resilience. the next optimization should decrease R_{p2}(surface passivation/co-adsorbents) without raising R_s, and future research should focus on refining the modification pathways, exploring hybrid sensitization strategies, and integrating multifunctional additives to concurrently enhance both efficiency and stability. By doing so, it will be possible to unlock the full potential of bio-inspired materials in next-generation, eco-sustainable photovoltaic technologies, paving the way for more durable, scalable, and commercially viable DSSC devices based on renewable organic dyes.

Acknowledgements The authors would like to express their gratitude to the Laboratory of Physical Chemistry of Interfaces of Materials Applied to the Environment at Blida 1 University, the Directorate General of Scientific Research and Technological Development, and the Institute for Chemical and Physical Processes (IPCF)—National Research Council (CNR), Viale Ferdinando Stagno D'Alcontres, Messina, Italy, for providing the necessary facilities, resources, and technical support for the electronic and mechanical apparatus used in the experimental setup. Special thanks are extended to the IPCF technical staff: Giuseppe Spinella, Giuseppe Lupò, Guerino Sarullo, Domenico Arigò and Roberto Caruso, for their valuable assistance. We acknowledge financial support by the European Union (NextGeneration EU), through the PNRR MUR project PE0000023-NQSTI and POR H2 AdP MMES/ENEA with involvement of CNR and RSE, PNRR - Mission 2, Component 2, Investment 3.5 "Ricerca e sviluppo sull'idrogeno", CUP: B93C22000630006.

Author contributions Investigation: A.C., Z.Z., Z.F., M.L., I.C., M.C., D.S., S.T., G.C. Methodology: A.C., C.B., Z.Z., Z.F., M.L., I.C., D.S., G.C. Data curation: A.C., S.T. Writing—original draft: A.C., C.B., Z.Z., M.C.,G.C. Writing—review and editing: A.C., C.B., Z.Z., M.L., D.S., S.T., G.C.Validation: A.C., Z.Z., G.C. Formal analysis: A.C., Z.Z., M.C., D.S., G.C. Conceptualization: C.B., Z.Z., G.C. Supervision: C.B., Z.Z., Z.F., G.C.Funding acquisition: C.B., Z.Z., Z.F. Project administration: C.B., Z.F., G.C. Resources: G.C. Visualization: G.C. All authors reviewed the manuscript.

Funding Open access funding provided by Consiglio Nazionale Delle Ricerche (CNR) within the CRUI-CARE Agreement.

Data availability No datasets were generated or analysed during the current study.

Declarations

Competing interests The authors declare no competing interests.

References

1. Hosseinnezhad, M., Nasiri, S., Nutalapati, V., Gharanjig, K., & Arabi, A. M. (2024). A review of the application of organic dyes based on naphthalimide in optical and electrical devices. *Progress in Color, Colorants and Coatings, 17*(4), 417–433. https://doi.org/10.30509/pccc.2024.167247.1267
2. Feng, T., Sun, Y., Shi, Y., Ma, J., Feng, C., & Chen, Z. (2024). Air pollution control policies and impacts: A review. *Renewable and Sustainable Energy Reviews*, *191*, 114071. https://doi.org/10.1016/j.rser.2023.114071
3. Shah, N., Shah, A. A., Leung, P. K., Khan, S., Sun, K., Zhu, X., & Liao, Q. (2023). A review of third-generation solar cells. *Processes*. https://doi.org/10.3390/pr11061852
4. Abdellah, I. M., & El-Shafei, A. (2020). Synthesis and characterization of novel tetra anchoring A_2-D-D-D-A_2 architecture sensitizers for efficient dye-sensitized solar cells. *Solar Energy, 198*, 25–35. https://doi.org/10.1016/j.solener.2020.01.040
5. O'Regan, B., & Grätzel, M. (1991). A low-cost, high-efficiency solar cell based on dye-sensitized colloidal TiO2 films. *Nature, 353*(6346), 737–740. https://doi.org/10.1038/353737a0
6. Kabir, F., Bhuiyan, M. M. H., Hossain, M. R., Bashar, H., Rahaman, M. S., Manir, M. S., Ullah, S. M., Uddin, S. S., Mollah, M. Z. I., Khan, R. A., Huque, S., & Khan, M. A. (2018). Improvement of efficiency of dye-sensitized solar cells by optimizing the combination ratio of natural red and yellow dyes. *Optik, 179*, 252–258. https://doi.org/10.1016/j.ijleo.2018.10.150
7. Saud, P. S., Bist, A., Kim, A. A., Yousef, A., Abutaleb, A., Park, M., Park, S., & Pant, B. (2024). Dye-sensitized solar cells: Fundamentals, recent progress, and optoelectrical properties improvement strategies. *Optical Materials, 150*, Article 1152.
8. Kumara, N. T. R. N., Lim, A., Lim, C. M., Mohamad, I. P., & Piyasiri, E. (2017). Recent progress and utilization of natural pigments in dye sensitized solar cells: A review. *Renewable and Sustainable Energy Reviews, 78*, 301–317. https://doi.org/10.1016/j.rser.2017.04.075.
9. Calogero, G., Di Marco, G., Cazzanti, S., Caramori, S., Argazzi, R., Di Carlo, A., & Bignozzi, C. A. (2010). Efficient dye-sensitized solar cells using red turnip and purple wild sicilian prickly pear fruits. *International Journal of Molecular Sciences, 11*(1), 254–267. https://doi.org/10.3390/ijms11010254.
10. Calogero, G., Yum, J., Sinopoli, A., Di Marco, G., Grätzel, M., & Nazeeruddin, M. K. (2012). Anthocyanins and betalains as light-harvesting pigments for dye-sensitized solar cells. *Solar Energy*, *86*(5), 1563–1575. https://doi.org/10.1016/j.solener.2012.02.018
11. Calogero, G., Bartolotta, A., Di Marco, G., Di Carlo, A., & Bonaccorso, F. (2015). Vegetable-based dye-sensitized solar cells. *Chemical Society Reviews*, *44*, 3244–3294. https://doi.org/10.1039/C4CS00309H
12. Barichello, J., Mariani, P., Matteocci, F., Vesce, L., Reale, A., Di Carlo, A., Lanza, M., Di Marco, G., Polizzi, S., & Calogero, G. (2022). The golden *Fig*: A plasmonic effect study of organic-based solar cells. *Nanomaterials, 12*(2), 267. https://doi.org/10.3390/nano12020267
13. Wu, J., Lan, Z., Lin, J., Huang, M., Huang, Y., Fan, L., & Luo, G. (2015). Electrolytes in dye-sensitized solar cells. *Chemical Reviews*, *115*(5), 2136–2173. https://doi.org/10.1021/cr400675m
14. Nastasi, F., Mineo, P. G., Barichello, J., La Ganga, G., Di Marco, G., Calogero, G., & Cordaro, M. (2022b). Synthesis and photophysical characterization of boronic styryl and distyryl BODIPYs for water-based dye-sensitized solar cells. *Biomimetics, 7*(3), Article 110. https://doi.org/10.3390/biomimetics7030110
15. Wu, M., & Ma, T. (2012). Platinum-free catalysts as counter electrodes in dye-sensitized solar cells. *ChemSusChem*, *5*(8), 1343–1357. https://doi.org/10.1002/cssc.201100676
16. Raj, C. C., & Prasanth, R. (2016). A critical review of recent developments in nanomaterials for photoelectrodes in dye sensitized solar cells. *Journal of Power Sources*, *317*, 120–132. https://doi.org/10.1016/j.jpowsour.2016.03.016
17. Hernandez-Martinez, A. R., Estevez, M., Vargas, S., Quintanilla, F., & Rodriguez, R. (2011). New dye-sensitized solar cells obtained from extracted bracts of *Bougainvillea glabra* and spectabilis betalain pigments by different purification processes. *International Journal of Molecular Sciences, 12*(9), 5565–5576. https://doi.org/10.3390/ijms12095565
18. Baxter, R., Hamsath, A., & Galloway, J. (2018). Quinone C–H alkylations via oxidative radical processes. *Synthesis*, *50*(15), 2915–2923. https://doi.org/10.1055/s-0037-1610005
19. Sturzoiu, A., Stoica, A., & Dobre, T. (2011). Betanine extraction from *Beta vulgaris*—Experimental research and statistical modeling. *UPB Scientific Bulletin, Series B: Chemistry and Materials Science, 73*, 1454–2331.
20. Azeredo, H. M. (2008). Betalains: Properties, sources, applications, and stability a review. *International Journal of Food Science & Technology, 44*(12), 2365–2376. https://doi.org/10.1111/j.1365-2621.2007.01668.x
21. Zhang, L., & Cole, J. M. (2015). Anchoring groups for dye-sensitized solar cells. *ACS Applied Materials & Interfaces*, *7*(6), 3427–3455. https://doi.org/10.1021/am507334m
22. Shaikh, R. S., Rajput, R. B., & Kale, R. B. (2024). Inexpensive green synthesis of natural dye-sensitized solar cells with aqueous solution as a Bi_2S_3 counter electrode. *Next Materials, 3*, 100051. https://doi.org/10.1016/j.nxmate.2023.100051
23. Seithtanabutara, V., Chumwangwapee, N., Suksri, A., & Wongwuttanasatian, T. (2023). Potential investigation of combined natural dye pigments extracted from ivy gourd leaves, black glutinous rice and turmeric for dye-sensitised solar cell. *Heliyon, 9*, Article e21533. https://doi.org/10.1016/j.heliyon.2023.e21533
24. Gómez-Ortíz, N. M., Vázquez-Maldonado, I. A., Pérez-Espadas, A. R., Mena-Rejón, G. J., Azamar-Barrios, J. A., & Oskam, G. (2010). Dye-sensitized solar cells with natural dyes extracted from achiote seeds. *Solar Energy Materials and Solar Cells*, *94*, 40–44. https://doi.org/10.1016/j.solmat.2009.05.013
25. Erande, K., Hawaldar, P., Suryawanshi, S., Babar, B., Mohite, A., Shelke, H., Nipane, S., & Pawar, U. (2020). Extraction of natural dye (specifically anthocyanin) from pomegranate fruit source and their subsequent use in DSSC. *Materials Today: Proceedings*, *43*, 2716–2720. https://doi.org/10.1016/j.matpr.2020.06.357
26. Yazie, N., Worku, D., & Reda, A. (2016). Natural dye as light-harvesting pigments for quasi-solid-state dye-sensitized solar cells. *Materials for Renewable and Sustainable Energy*. https://doi.org/10.1007/s40243-016-0077-x
27. Hemalatha, K., Karthick, S., Raj, C. J., Hong, N., Kim, S., & Kim, H. (2012). Performance of *Kerria japonica* and *Rosa chinensis* flower dyes as sensitizers for dye-sensitized solar cells. *Spectrochimica Acta Part A: Molecular and Biomolecular Spectroscopy, 96*, 305–309. https://doi.org/10.1016/j.saa.2012.05.027